Isotopic effect of oxygen on the Raman mapping of a polycrystalline uranium dioxide UO2

Clotilde Gaillard, Lola Sarrasin, Clémentine Panetier, Yves Pipon, Roland Ducher, Nathalie Moncoffre

Isotopic effect of oxygen on the Raman mapping of a polycrystalline uranium dioxide UO_2

C. Gaillard[a*], L. Sarrasin[a], C. Panetier[a], Y. Pipon[a,b], R. Ducher[c], N. Moncoffre[a]

[a] Univ Lyon, Univ Claude Bernard Lyon 1, CNRS/IN2P3, IP2I Lyon, UMR 5822, F-69622, Villeurbanne, France

[b] Univ Lyon, UCBL, IUT Lyon-1, Département chimie, F-69622, Lyon, France

[c] IRSN, LETR – BP3 13115 St-Paul-Lez-Durance Cedex, France

* corresponding author: gaillard@ipnl.in2p3.fr

Abstract (250 mots max)

Uranium dioxide UO_2 is a widely studied material due to its use as fuel in Pressurized Water Reactors (PWR) and Raman spectroscopy is a technique of choice to characterize the evolution of its microstructure. UO_2 crystallizes in a fluorite CaF_2 (space group Fm-3m) structure that gives rise to a unique Raman signature, the T_{2g} band. However, several other bands are often detected whose attribution remains unclear. The present study gives new insights on the Raman spectrum of UO_2 thanks to the combination of isotopic labelling with ^{18}O and Raman imaging. In addition to the expected T_{2g}, U_2 (LO), 2LO and U_3 bands, we have detected a doublet at 885 and 925 cm^{-1}, a U* band at 555 cm^{-1} in some specific areas and 2 bands located at 367 and 1196 cm^{-1}. All Raman bands shift under the effect of the replacement of ^{16}O by ^{18}O, excepting for the U* band that could not be detected anymore. The isotopic shift ratio could be determined for 20% and 30% ^{18}O labelling. No discrepancy in band position is observed between grains and grain boundaries, except for the U_2(LO) band. We also evidence a difference between the U defect bands and the 885 and 925 cm^{-1} doublet bands evolution under labelling, although the latter also seems to be connected to the presence of defects in the material.

Keywords

UO_2, oxygen labelling, Raman mapping

1. Introduction

Uranium dioxide UO_2 is a material widely studied due to its use as fuel in PWR nuclear reactors. The knowledge of its behaviour in reactor is of crucial importance, in normal operation but also in the case of incidental or accidental operations[1]. The release of fission products out of nuclear fuel is often correlated to the fuel microstructure evolution under high temperature, irradiation and oxidation[2-5]. However polycrystalline UO_2 is not a homogeneous material with the existence of zones with different crystallinities such as grains and grain boundaries. Therefore, getting information at the micrometre scale is mandatory to improve the modelling of nuclear fuel in operation. Raman spectroscopy is a technique of choice to study UO_2. This material crystallizes in a fluorite CaF_2 (space group Fm-3m) structure that gives rise to a unique Raman signature.[6] Raman spectroscopy was shown to be a powerful tool to study the structure of UO_2 or mixed An oxides [7-12] under irradiation [13-19] or under oxidation[20-27]. However, the limit of Raman spectroscopy for nuclear fuel studies is the lack of

unambiguous interpretation of the bands observed in the spectrum of UO_2. Indeed, the Raman spectrum of UO_2 contains very often more peaks than the unique Raman mode T_{2g} predicted by group theory at 445 cm^{-1}.[28] Between 500 and 700 cm^{-1}, several bands may be observed: the U_2 and U_3 bands are always present with more or less intensity, while a U_1 band at ~530 cm^{-1} is mainly observed in doped UO_2 or irradiated UO_2. It is commonly accepted that the U_2 band corresponds to a LO infrared forbidden mode activated by the presence of defects in the material while the band observed at 1150 cm^{-1} would be an overtone of the LO band. Nevertheless, the origin of the other bands remains unclear. The situation is even more complex as another "defect" band is sometimes present, the so-called U*. In this context, the present study gives new insights on the Raman spectrum of UO_2 thanks to the combination of isotopic labelling with ^{18}O and Raman imaging. Isotope exchange is a common technique used in conjunction with vibrational spectroscopy techniques as a mean of identifying the number and types of vibrations in a material. Isotope substitution is a unique tool for distinguishing different Raman active modes, and it can lead to a reliable assignment because only vibrations involving the motion of the substituted ion will be shifted.[29-31] Raman spectroscopy is sensitive to the isotopic composition of the material examined. This arises due to the dependence of the vibrational frequency on the mass of the atoms involved. Therefore, isotopic substitution is reflected in the Raman spectra as a shift in the spectral bands upon incorporation of different isotopes into a vibrating group. The present study aims to use the capability of Raman imaging with a high spatial resolution (about 1 µm) that can provide insight on the heterogeneities within the sample surface and shed some light on their origin.[32]

2. Materials and methods

Sample preparation

Depleted UO_2 pellets (0.3% ^{235}U, 8.9 mm diameter and 1.6 mm thick) provided by Framatome were sintered at 1750°C under hydrogen. They have a high density (97.5% of the theoretical density) and an average grain size of 11 microns. The pellets were polished by PrimeVERRE (Montpellier, France) with diamond paste and annealed twice: at 1000°C under vacuum for 10 hours and then at 1600°C under a reducing gas mixture (5% H_2/Ar) for 4 hours. Both annealing treatments are used to eliminate adsorbed impurities, polishing defects and ensure a stoichiometric composition UO_2. [33,34]

Labelled water with ^{18}O isotope at a controlled concentration was prepared by dilution of ^{18}O labelled ultra-pure water (97% ^{18}O, Sigma Aldrich) with deionized water (resistivity 18.2 MΩ.cm, natural abundance of ^{18}O = 0.205 at.%). The error on the final ^{18}O concentration, calculated considering the error on the volume uptakes, was below 1%.

In order to label stoichiometric UO_2 with ^{18}O, UO_2 pellets were annealed for 10 hours at 950°C in a wet atmosphere in a tubular furnace. The oxygen partial pressure (pO_2) in contact with UO_2 pellet was fixed at $3x10^{-15}$ atm using H_2/Ar gas bubbling into ^{18}O labelled water. This oxygen partial pressure results in a ΔG = -340 kJ/mol, which means that the UO_2 oxidation is expected to be negligible under these conditions (~ $UO_{2.001}$ at maximum).[35] The ^{18}O concentration in the samples was adjusted by fixing the ^{18}O concentration in the labelled water used to produce oxygen in the furnace atmosphere. SIMS analyses were used to measure the isotopic oxygen ratio in the samples (see Figure S1, Supplementary Information). They also show that, under our experimental annealing conditions, the diffusion of oxygen 18 occurs at least over the first 100 µm of the pellet and that its concentration can be considered as constant over the first 5 µm, which is above the depth probed by Raman spectroscopy[36].

Raman spectroscopy

Raman spectroscopy analyses were performed at 20°C on a Renishaw Invia Qontor using a He-Ne laser (633 nm) equipped with a grating 1800 gr/mm to achieve a spectral resolution of 0.4 cm^{-1}. A great care has been taken to ensure that the laser does not induce any structural modifications during the measurements, using a laser power of 1 mW. Raman mappings were performed on the surface of UO_2 pellets with a 50x objective, with a spatial resolution of 1x1 µm². The laser spot size was ~1 µm². Each analysis covers at least 10 grains while the depth probed is estimated to be between 3 and 5 µm.[37] As a result, each map consists in several thousand Raman spectra. Mapping allows the visualization of a chosen parameter (position, intensity, width of a chosen Raman band) which can be extracted by fitting procedure. In our case, band fitting was performed using the WIRE 5.0 software with Gaussian-Lorentzian curves, excepting for the T_{2g} band fitted with a pure Lorentzian curve. The interest of such mappings is to evidence heterogeneities as a function of grains and grain boundaries for a given Raman band, and to allow the comparison of intensity features between bands. We have also extracted an averaged Raman spectrum by merging the set of spectra measured during mapping.

3. Results and discussion

3.1. UO_2 Raman spectrum

Figure 1 displays the Raman spectrum of a stoichiometric UO_2 pellet (containing only ^{16}O), obtained between 200 and 1300 cm^{-1}. This spectrum, background subtracted, is an average of several thousand spectra measured on a zone covering several grains (~120 µm x 80 µm), whose optical microscopy image is shown on Figure 2. The average spectrum before background removal is presented in Figure S2 (Supplementary Information). One can see that the Raman intensity is noticeable after 1200 cm^{-1} which is due to the presence of several bands after 1200 cm^{-1}.[38] It was not possible to perform mappings on a larger spectral range, so the background removal procedure does not take them into account. It has no consequences on most of the spectrum, excepting after 1100 cm^{-1}. However, as will be discussed later, it does not entail significant inaccuracies in our results.

Eight Raman bands can be identified on each spectrum at ~367, 445, 574, 619, 885, 925, 1146 and 1196 cm^{-1} and a ninth at 555 cm^{-1} on some specific areas. The most intense one, centred at 444.8 ± 0.2 cm^{-1}, corresponds to the T_{2g} band. The existence of this Raman-active vibrational mode is predicted by the group theory as it comes from the face-centred cubic unit cell of UO_2 fluorite structure.[39] The position of the T_{2g} band is expected to be independent of the crystalline orientation of UO_2 crystals, so its position should not vary between grains. As a matter of fact, the T_{2g} position variation on our mapping is not significant (± 0.2 cm^{-1}). The T_{2g} band width, which is related to the presence of defects in the fluorite structure,[18] is also very homogeneous on the whole analysed area (FWHM = 15.8 ± 0.2 cm^{-1}). The T_{2g} area map at the surface of the pellet is displayed on Figure 2, it is identical to the T_{2g} intensity map (not shown). As observed in ref [40], the area and intensity of this band depends on grains, which is due to the different crystalline orientations of UO_2 grains that respond differently to the fixed polarization of the incoming and outgoing light.[41]

On Figure 1, we observe at the bottom left of the T_{2g} peak a small peak at 367 cm^{-1}. It was also evidenced by Maslova et al. and Livneh on a pristine UO_2 pellet.[37,38] The latter author attributes it to 2 longitudinal modes $LO_R(L)$+LA(L). The position of this band could be evaluated but its fit was not possible because of its low intensity and its presence at the bottom of the very intense T_{2g} peak.

The large peak visible between 1100 and 1200 cm^{-1} is better fitted using two contributions: a large band centred at 1146 cm^{-1}, which corresponds to the expected 2LO band, and another small band located at 1196 cm^{-1}. The origin of the 2LO band has been the subject of many discussions. Initially, it was attributed to crystal field transition.[20,42,43] However, this assignment has been questioned by Livneh and Sterer [44] who consider the band as an overtone (2LO) of the first order LO phonon (575 cm^{-1}) band. It was further confirmed by Elorrieta et al. [45] The band at 1196 cm^{-1} may correspond also to a 2LO mode. In a recent work, Livneh analysed a UO_2 sample at 77 K using a 532 nm laser, with a wider spectral range up to 2300 cm^{-1}.[38] He evidenced several bands in the 1000-2200 cm^{-1} region. In particular 2 bands under the "2LO" band are attributed to two different 2LO modes: the intense band at 1147 cm^{-1} (usually denominated as the "2LO band") is attributed to a 2LO(Γ) mode and a second band at 1181 cm^{-1} is attributed to a 2LO(L) mode. For sake of comparison, we have measured a Raman spectrum of UO_2 in an extended mode, up to 2500 cm^{-1}. It is displayed in Figure S3. Fit of the 800-2500 cm^{-1} region is also shown. The 2 bands located at 1146 cm^{-1} and 1196 cm^{-1} on the mapping (obtained up to 1300 cm^{-1}) are located respectively at 1145 and 1190 cm^{-1} considering a wider spectral range and the presence of further bands in this region. So, there is a slight effect of the spectral range on the 1196 cm^{-1} band position. This latter band may correspond to the 1180 cm^{-1} band attributed to a 2LO(L) mode by Livneh. The difference in band position may be easily explained by the number of bands used to fit the spectrum. Indeed, we do not evidence as many bands above 1200 cm^{-1} than Livneh, as our spectrum was measured under different experimental conditions, i.e. at ambient temperature with a red laser.

On the mapping, the position of the 2LO(Γ) and 2LO(L) at 1146 and 1196 cm^{-1} is quite homogeneous on the surface (± 0.7 cm^{-1} and ± 1.0 cm^{-1}) as well as their widths (61.4 ± 0.4 cm^{-1} and 43 ± 3 cm^{-1}) and areas. So, contrary to the T_{2g} band, these bands area cannot be correlated with the morphology of the UO_2 pellet.

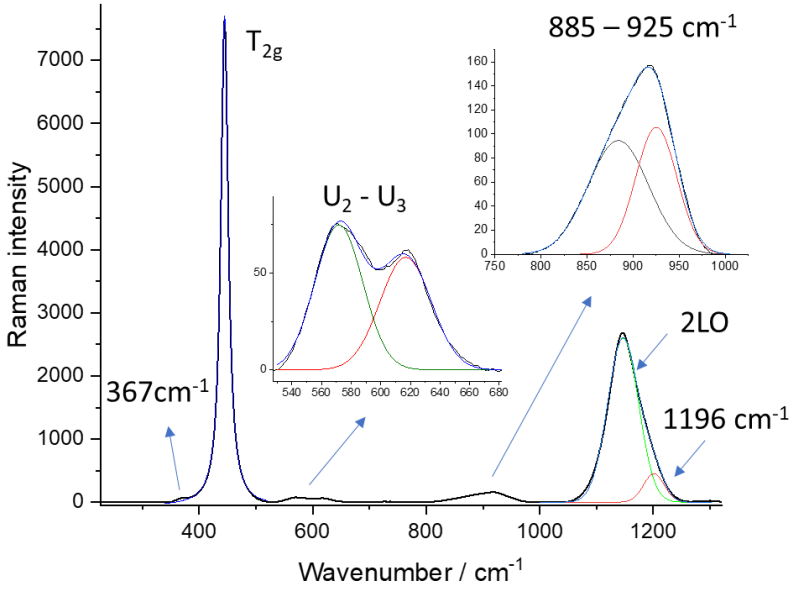

Figure 1: Raman spectrum of pristine UO_2, obtained by an average of 10500 spectra measured at the surface of the sample (cf. optical picture on Figure 2).

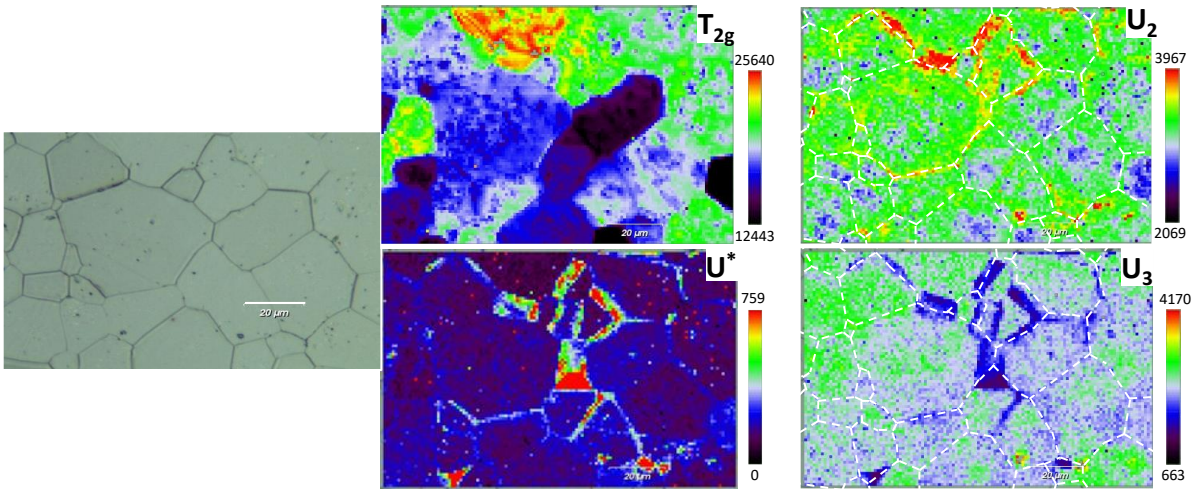

Figure 2: Mappings of the different Raman band areas at the surface of a pristine UO_2 pellet: T_{2g}, U, U_2, U_3. Colours correspond to a scale of intensity, from black to red as the area increases. For sake of clarity, grain boundaries visible on the optical picture are represented by white dotted lines on some maps.*

The presence of a peak doublet is detected in the 500-700 cm^{-1} region, at 572 cm^{-1} and 619 cm^{-1} according to the fit of the average Raman spectrum. We can ascribe it to the so-called U_2 (LO) and U_3 bands. These two bands were correlated to the presence of defects in the UO_2 crystallographic structure[46] and to the formation of domains with a local symmetry lower than the one of perfect UO_2.[47] Their low intensity indicates that our polycrystalline UO_2 samples are well-structured, which is expected after the thermal treatment at 1600°C under reducing atmosphere. The average position of U_2 over the whole sample is 572 cm^{-1}, but this value hides big discrepancies. Figure 3 shows the evolution of this band position at the surface of the UO_2 pellet. Inside grains, U_2 is located at a mean value of 572 ± 1 cm^{-1} (in green on the mapping). There are also small, well-defined areas appearing in dark blue on the mapping, where U_2 is located at ~565 cm^{-1}. An explanation for this low value can be found comparing the individual spectra measured in a grain (green zone of the mapping) and those measured in the dark area in the mapping. One of each is displayed in Figure 3. Inside grains, the 500-700 cm^{-1} region is well fitted using only U_2 and U_3 bands positioned respectively at 572 ± 1 and 617 ± 1 cm^{-1}. In the dark zone of the mapping, the best fit is obtained by adding a third band which is found centred at ~555 cm^{-1}, while U_2 and U_3 bands are located respectively at 573 ± 1 and 619 ± 1 cm^{-1}. According to the fitted position of this additional band, we have ruled out the hypothesis that it could be the so-called U_1 band, detected around 530 cm^{-1} in irradiated or doped UO_2 materials.[14] This defect band at 555 cm^{-1} ("U* band") was observed by several authors and is usually associated with grain boundaries.[37,44,46] In our case, the U* band is intense in specific areas of the surface that correspond only partly to grain boundaries, other areas may correspond to underlying grains (cf. Figure 2). It is possible to detect Raman signal from such underlying grains as the depth of analysis of Raman spectroscopy at the 633 nm wavelength is estimated to range between 3 and 5 µm. Thus, it appears that the U* band is not specific of grain boundaries, but probably to the presence of zones with lower strains than in grains. Livneh evidenced a 2TO(Γ) band at 550 cm^{-1} in UO_2 spectrum, using a green laser

(532 nm). As our measurements were made using a different wavelength excitation, we cannot firmly state whether our U* band, observed using a 633 nm laser, can be attributed to this 2TO(Γ) mode.

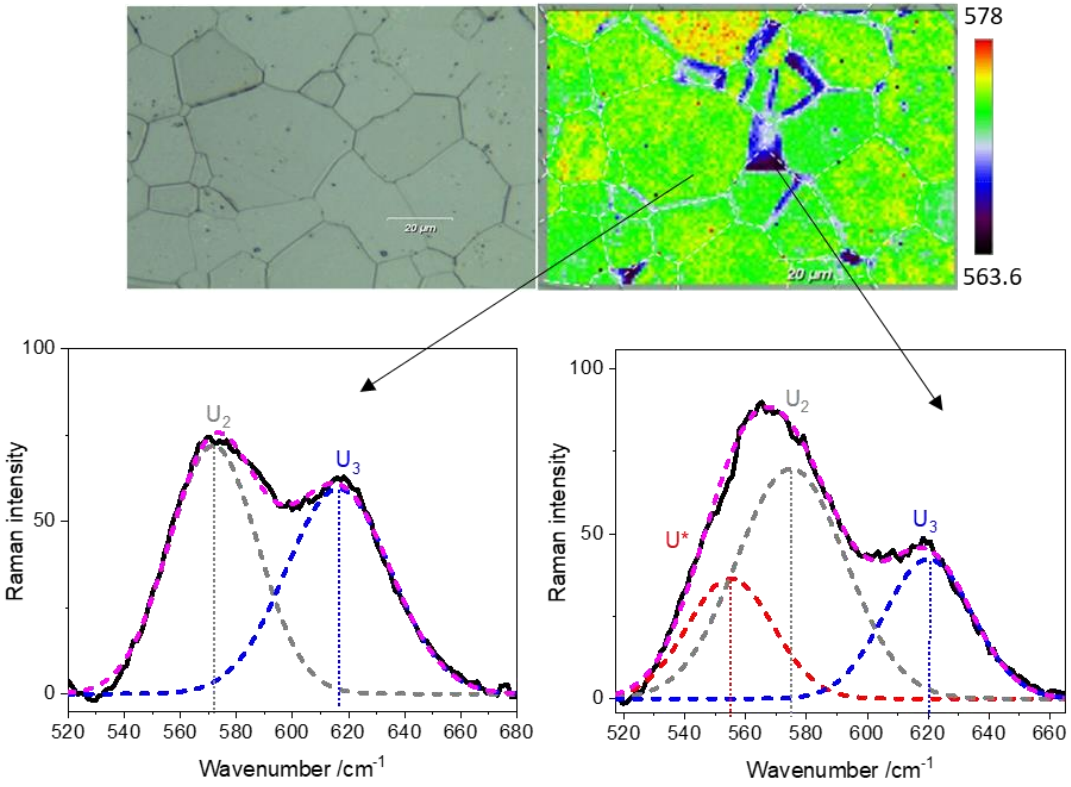

Figure 3: At the top, mapping of U_2 band position on pristine UO_2, obtained by fitting the 500-700 cm^{-1} region using the U_2 and U_3 bands. For sake of clarity, grain boundaries visible on the optical picture (left) are represented as white dotted lines on mapping. Below, comparison of Raman spectra measured in the green area (left) or in the black area (right) of the mapping.

The evolution of U_2 and U_3 band area at the surface of the UO_2 pellet is displayed on Figure 2. The area of U_3 is quite homogeneous at the sample surface, but is less intense in the zones where the U* band is present. The U_2 band seems to be more intense in some grain boundaries. The origin of these bands has already been discussed in the literature. The U_2 band is attributed to a loss of symmetry in the fluorite structure that would activate the forbidden mode LO. This is consistent with the fact that it is more intense in grain boundaries, a region where the crystallinity is lower. The U_3 band is intense in hyper-stoichiometric UO_{2+x} samples and in U_4O_9 [23,48] and it was also observed after irradiation.[18,46] For these reasons, it was attributed to a distortion of the oxygen sublattice.

On the UO_2 Raman spectrum shown in Figure 1, we also notice the presence of a weak contribution between 800 and 1000 cm^{-1}. It corresponds to a peak doublet centred respectively at 885 and 925 cm^{-1}. The presence of bands in the 800-900 cm^{-1} region was observed by Talip et al. on a UO_2 pellet and was attributed to uranyl ion-containing phases, formed by a slight air oxidation on the surface of UO_2.[8] In our study, this explanation can be ruled out for several reasons. First, Raman analysis was performed just after the UO_2 pellet had been submitted to an annealing treatment under

reducing atmosphere that would have reduced any uranyl-oxide phases. Also, the position of the two bands detected in our sample does not match the position of the uranyl (UO_2^{2+}) signature at ~820-840 cm^{-1}, nor the position of typical oxide phases like studtite or schoepite at ~870 cm^{-1}.[15,31,49-52] It must be noted that Livneh et al. have detected a band at 918 cm^{-1} on a UO_2 pellet that was attributed to a $2TO_R(X)$ mode [44]. Senanayake et al. [53] have also detected an unassigned band at 930 cm^{-1} on a UO_2 single crystal analysed with a 488 nm excitation source. The area mapping of these two bands at the sample surface is homogeneous. However, if we plot the evolution of their area as a function of the (U_2+U_3) bands area, normalized to the T_{2g} band area (Figure 4, black dots), we evidence a linear correlation between the two families of bands. Considering that U bands occur from the presence of defects in the UO_2 microstructure, we can assume that these bands centred at 885 and 925 cm^{-1} have the same origin.

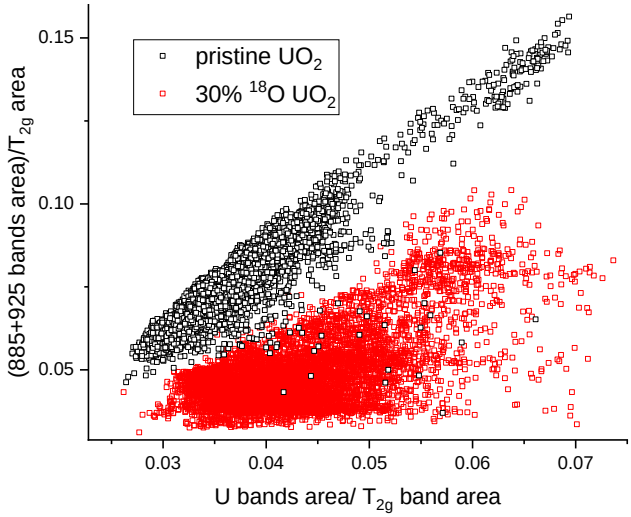

Figure 4: Evolution of the 885-925 cm^{-1} doublet area as a function of the U bands area, normalized to the T_{2g} area. In black, for the pristine non labelled UO_2 and, in red, for the 30% ^{18}O labelled UO_2.

3.2. Effect of ^{18}O labelling on the Raman spectrum of UO_2:

In order to label UO_2 with ^{18}O, we have performed a thermal treatment by submitting samples to an annealing at 950°C under a wet atmosphere (^{18}O labelled H_2O at 20% and 30% + Ar/H_2). Prior to the experiments using ^{18}O labelled water, we have checked that the thermal treatment itself does not change the UO_2 microstructure by using unlabelled water vapor ($H_2{}^{16}O$). We found no changes between the pristine UO_2 and 0% ^{18}O annealed samples on the XRD spectra (same lattice parameter, no additional crystallographic phase) nor on the Raman signature, the same bands (including the U*) being measured at the same positions (cf. Figure 5). This thermal treatment entails a slight increase of the U_2 and U_3 band intensity that could reveal an increase of defect concentration in the material. However, this tendency is not assessed by a widening of the T_{2g} band whose width remains identical before and after the thermal treatment (16.0 cm^{-1}). A very slight decrease of the "2LO bands" peak (i.e. 2LO(Γ) and 2LO(L) bands) is also observed.

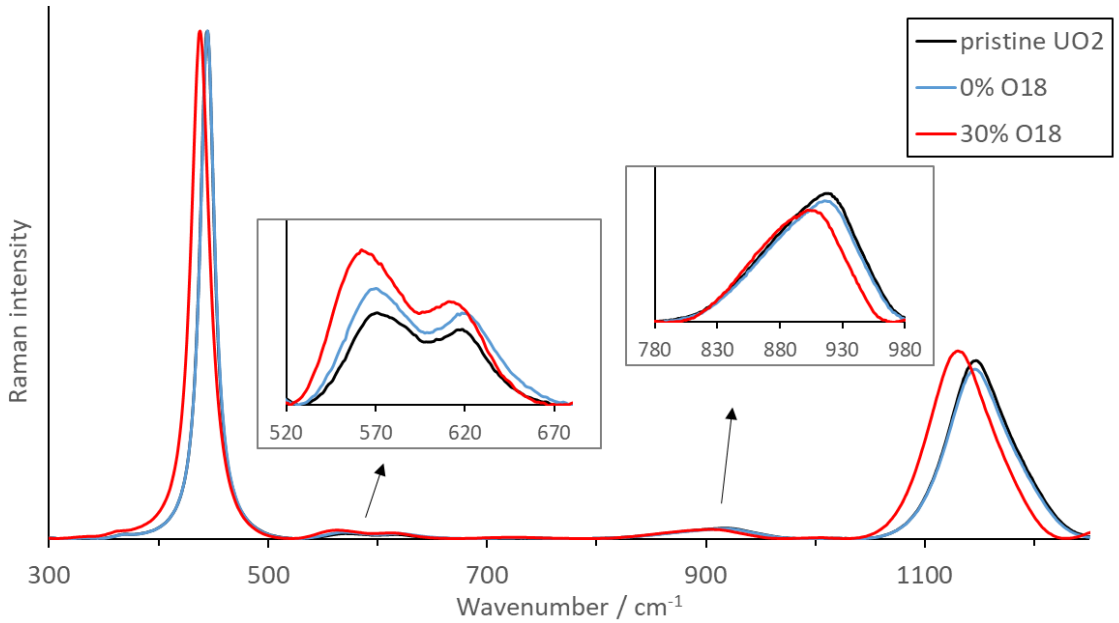

Figure 5: Comparison of the Raman spectra of a pristine UO_2 (black), a UO_2 pellet containing 30% of ^{18}O (red) and a pellet submitted to the labelling thermal treatment with 0% of ^{18}O (blue). Spectra were obtained by merging several thousand spectra of surface mapping. Background removal was performed after average. See in Figure S2 (Supplementary Information) those spectra before background removal. For sake of comparison, spectra were normalized to the T_{2g} band intensity.

The isotopic exchange between ^{16}O and ^{18}O up to 30% does not change the overall shape of the Raman spectrum of UO_2, as can be seen on Figure 5. The main visible effect of the ^{18}O labelling is the significant redshift of all band positions. This phenomenon was evidenced by Lv et al. [54] on the T_{2g}, U_2 and 2LO bands in UO_2 powder containing 98% of ^{18}O. In our experiment, this is very clear on the T_{2g} band, whose average position shifts from 444.8 to 438.2 cm^{-1}. The T_{2g} band is a symmetric breathing mode of O ions around a static U ion. Its position is not sensitive to defects in the material as long as the UO_2 stoichiometry and lattice parameters are preserved, as in our experiment. Therefore, the T_{2g} position shift can be ascribed to the sole isotopic effect. On the mapping (not shown), the T_{2g} position varies at the surface of the samples within uncertainties: between 444.7 to 444.9 cm^{-1} before labelling, between 438.0 to 438.4 cm^{-1} after 30% ^{18}O labelling. A significant broadening (+ 4 cm^{-1}) of the T_{2g} band is observed under the effect of labelling, that is now measured at 20.2 ± 0.2 cm^{-1}. It must be noticed that this broadening is symmetric and we do not evidence the presence of any other band under the T_{2g} band, like the so-called U_4 band evidenced at ~460 cm^{-1}.[47] The T_{2g} broadening is very homogeneous at the surface of the sample. The homogeneity of the T_{2g} position and width over the sample allows to consider that the isotopic labelling is homogeneous in the analysed depth of the sample.

By comparison with mappings in pristine UO_2 (Figure 2), the isotope exchange does not affect the global repartition of bands at the surface (cf. Figure S4 in Supplementary Information): the T_{2g} band area still depends on grains and their crystallographic orientations; U_2 and U_3 bands are present on the whole mapping. Other bands (not shown: 2LO(Γ), 2LO(L), 885 and 925 cm^{-1}) exhibit the same homogeneous mapping at the sample surface. However, some evolution on the band area with respect to the T_{2g} one is observed. For the U_2 and U_3 bands, the U/T_{2g} area ratio increases significantly after

the ^{18}O labelling process (respectively +60% and +70%), only part of it can be attributed to the thermal treatment itself. This increase, in agreement with the T_{2g} band broadening, confirms that the isotopic exchange produces significant number of defects (vacancies/interstitial ions) that would require much higher temperature than 950°C to be annealed. It is interesting to note that the 885-925 doublet band area displays the opposite tendency than the U bands, with a noticeable area decrease after isotopic exchange (~-25%). The quasi-linear evolution of the doublet bands vs. U bands, observed before labelling, is also less clear after labelling (red dots in Figure 4). Finally, the 2LO(Γ) band area, with respect to the T_{2g} one, does not change after the labelling. This latter observation indicates that this band is less sensitive than the LO band to the presence of defects in UO_2, which confirms previous studies.[44]

Figure 6 presents the evolution of the U_2 band position on the labelled ^{18}O sample, obtained by fitting the 500-700 cm^{-1} region using two bands (U_2 and U_3). The U_2 position on the overall mapping goes from 559 to 568 cm^{-1} (mean value = 564 cm^{-1}). We clearly see that the lowest positions (559-563 cm^{-1}) correspond mainly to grain boundaries while the U_2 position in grains is found between 563 and 568 cm^{-1}. At the same time, we could not detect any U* band in the grain boundary region, the ^{18}O isotopic labelling has entailed its disappearance in the sample. Figure S5 (Supplementary Information) compares individual spectra measured in a grain and in a grain boundary. Both are well fitted using only U_2 and U_3 bands, the sole difference being the U_2 position, at 560 cm^{-1} in grain boundaries while it is located at 565 cm^{-1} inside grains. It must be noticed that except for the U_2 band, we did not evidence any significant difference in band positions between grain and grain boundaries on mappings.

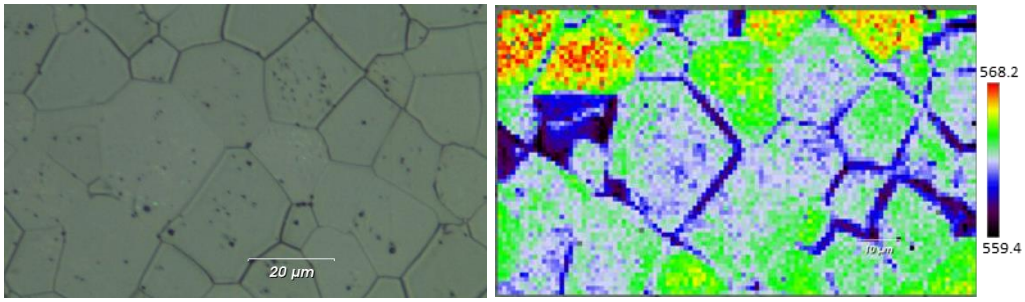

Figure 6: Evolution of U_2 band position at the surface of a 30% ^{18}O labelled UO_2 pellet. Colours correspond to the scale of wavenumber, from black (lowest value at 559 cm^{-1}) to red (highest value at 568 cm^{-1}).

The shift of each band position, obtained from the fit of averaged spectra of UO_2 pellets labelled with 20% and 30% of ^{18}O, is displayed in Figure S6 (Supplementary Information). All bands shift linearly with the oxygen 18 concentration. Data of Lv et al. obtained on UO_2 powder enriched with 98% of ^{18}O have been added and we see an excellent agreement with our results. Raman active modes are due to specific ion vibrations and the isotopic substitution will lead to a band shift only when the new isotope participates to the vibration. As a consequence, a band will not shift if it is due to purely electronic effects. It is therefore clear that all bands observed in UO_2 spectra between 300 and 1200 cm^{-1} have a vibrational origin.

The isotopic shift ratio, *i.e.* the ratio between the band position in ^{16}O UO_2 (ω_{16O}) and its position in the ^{18}O labelled UO_2 (ω_{18O}), depends mainly on the concentration of the new isotope, but also on the effective mass of each Raman mode, *i.e.* on the nature of the vibration. For this reason, it may differ

from band to band, as observed for the experimental shift ratio determined in our experiments (Table 1). It is also possible to calculate the theoretical isotopic shift of the T_{2g} and U_2(LO) band positions, using the equations established by Shimanouchi [55] and Lv [54]. The T_{2g} position is inversely proportional to the square root of the oxygen atom mass (taking into account the ^{18}O %) while the U_2(LO) position is proportional to the square root of the reduced mass (taking into account O and U atoms). The calculated isotopic shift ratio for a 30% ^{18}O doped UO_2 is 1.019 for the T_{2g} band and 1.017 for the LO band. These theoretical values are very close, although higher, than the experimental ones, as observed also by Lv.[54]

The isotopic shift ratio induced by ^{18}O is identical within two groups of data. In the first group (T_{2g}, U_2, 2LO and the 1196 cm^{-1} bands), it is equal to 1.014-1.015. These bands correspond to well-identified vibration modes. The second batch of bands (U_3, 885 and 925 cm^{-1} bands) has a significantly lower experimental shift ratio (1.010-1.011). The U_3 band is usually attributed to a distortion of the oxygen atom sub-network by the presence of interstitial oxygen clusters, leading to the formation of local hyper-stoichiometric zones in UO_2 lattice. Thus, one might expect a larger sensitivity of U_3 to the ^{18}O labelling than for other bands, which is not the case. Even if the sensitivity of this band to oxidation has been demonstrated, one may conclude that phenomena behind its presence are more complex than expected.

Table 1: Comparison of UO_2 band positions (obtained by fitting the average spectrum of mapping) and experimental isotope shift ratio for a pristine UO_2 sample and a UO_2 sample labelled with 30% ^{18}O.

band	Position ω (cm^{-1})		Isotopic shift ratio (30% ^{18}O)
	Pristine UO_2	30% ^{18}O	$\omega_{16O}/\omega_{18O}$ (±0.001)
367 cm^{-1}	367	362	1.014
T_{2g}	444.8	438.2	1.015
U_2 (LO)	572	564	1.014
U_3	617	611	1.010
885 cm^{-1}	885	876	1.010
925 cm^{-1}	925	915	1.011
2LO(Γ)	1146	1130	1.014
2LO(L)	1196	1180	1.014

4. Conclusion

We have performed a detailed Raman analysis of stoichiometric UO_2 pellets and characterized the effect of ^{18}O labelling on the Raman signature. For this purpose, we performed mappings at the surface of UO_2 samples, covering at least 10 grains and an estimated depth of 3 to 5 µm, which allows visualising the Raman band position, width or area and hence evidencing possible correlation with these features and the sample morphology (like grains or grain boundaries). In addition to the commonly detected T_{2g}, U_2 (LO), U_3 and 2LO bands, we have also detected additional bands. In the 500-700 cm^{-1} region, a U* band at 555 cm^{-1} is present in some specific areas. A small band is present at 367

cm^{-1}, attributed to $LO_R(L)$+LA(L) modes. We have also noticed the presence of two bands, located at 885 and 925 cm^{-1}. Finally, the fit of the "2LO band" between 1050 and 1250 cm^{-1} reveals the presence of an additional band at 1196 cm^{-1} that may correspond to a 2LO(L) mode.

The replacement of ^{16}O by ^{18}O induces a shift in the position of Raman bands involving vibrations of the new isotope. This is clearly observed for the eight bands detected in UO_2 after labelling. We do not observe any discrepancies between grain and grain boundaries, except for the U_2 band. Indeed, the U_2 band position is significantly lower in grain boundaries, a tendency also observed at a lesser degree in pristine UO_2. One may associate this phenomenon with the particular nature of grain boundaries. The latter contain a high concentration of defects like dislocations that entails a lower crystallinity, and probably, tensile strains. Some kind of strains may also be involved in the presence of the U* band. This U* band, located at ~555 cm^{-1}, is usually described in the literature as being specific to grain boundaries. In our experiments, it is present in some grain boundaries (not all of them) but also in zones corresponding to the presence of underlying grains. Interestingly, the introduction of ^{18}O in UO_2 entails a disappearance of the U* band, a phenomenon that cannot be ascribed to the defect annealing by the thermal treatment at 950°C.

The largest isotopic shift ratios (1.014-1.015) entailed by ^{18}O labelling are measured for the T_{2g}, U_2 (LO), 2LO, 367 and 1196 cm^{-1} bands. The 2LO band area is negligibly sensitive to the thermal treatment nor to the ^{18}O labelling. On the opposite, the U_2 and U_3 bands are more intense after the thermal treatment, a tendency enhanced in presence of ^{18}O. We thus confirm previous observations showing that although the U_2(LO) and 2LO(Γ) bands arise from the same origin (Fröhlich interactions), the U_2(LO) is also strongly affected by defects and is a good indication of disorder in UO_2.

The U_3 and 885-925 cm^{-1} bands exhibit the smaller ratio (1.010-1.011). The U_3 band is usually attributed to the formation of local hyper-stoichiometric zones in UO_2 lattice. Thus, one might expect a larger sensitivity of U_3 to the ^{18}O labelling than for other bands, which is not the case. The origin of the doublet at 885-925 cm^{-1} is not attributed even if we evidence that it implies the vibrations of oxygen ions. Their area ratio normalized to the T_{2g} band evolves linearly vs. the U defect bands in pristine UO_2. So, we may think that this doublet arises also from defects present in the material. However, we observe its decrease with the labelling, which is shown to produce defects as the U bands area increase in conjunction with the T_{2g} band widening. It means that the vibrations leading to the presence of this doublet were partly inhibited. We can make the hypothesis that if the presence of the doublet at 885-925 cm^{-1} is linked with the presence of defects in the materials, these defects may be of a different nature than the ones involved in the U bands, or that they correspond to different vibrational processes involving resonant interactions. One may also suggest that these 2 modes are second order modes.

Acknowledgements

The authors would like to thank Raphael Fillol (IP2I) for his helpful technical contribution. We acknowledge Denis Mangin (IJL, Nancy, France) for SIMS analysis.

CONFLICT OF INTEREST

On behalf of all authors, the corresponding author states that there is no conflict of interest.

DATA AVAILABILITY STATEMENT

The datasets generated and analysed during the current study are available from the corresponding author upon reasonable request.

References

[1] M. Barrachin, D. Gavillet, R. Dubourg, A.D. Bremaecker *J. Nucl. Mater.* **2014**, *453*, 340.
[2] E. Geiger, C. Le Gall, A. Gallais-During, Y. Pontillon, J. Lamontagne, E. Hanus, G. Ducros *J. Nucl. Mater.* **2017**, *495*, 49.
[3] J.-P. Hiernaut, T. Wiss, D. Papaioannou, R. Konings, V. Rondinella *J. Nucl. Mater.* **2008**, *372*, 215.
[4] C. Le Gall, F. Audubert, J. Lechelle, Y. Pontillon, J.-L. Hazemann *EPJ Nuclear Sci. Technol.* **2020**, *6*, 2.
[5] L. Sarrasin, C. Gaillard, C. Panetier, Y. Pipon, N. Moncoffre, D. Mangin, R. Ducher, M. Dubourg *Inorg. Chem.* **2019**, *58*, 4761.
[6] D.H. Lin, D. Manara, P. Lyndqyist-Reis, T. Fanghanel, K. Mayer *Vib. Spectrosc.* **2014**, *73*, 102.
[7] Z. Talip, S. Peuget, M. Magnin, L. Berardo, C. Valot, R. Vauchy, C. Jégou *J. Raman Spectrosc.* **2017**, *48*, 765.
[8] Z. Talip, T. Wiss, P.E. Raison, J. Paillier, D. Manara, J. Somers, R.J.M. Konings *J. Am. Ceram. Soc.* **2015**, *98*, 2278.
[9] A. Milena-Perez, L.J. Bonales, N. Rodriguez-Villagra, S. Fernandez, V.G. Baonza, J. Cobos *J. Nucl. Mater.* **2021**, *543*, 152581.
[10] F. Lebreton, D. Horlait, R. Caraballo, P.M. Martin, A.C. Scheinost, A. Rossberg, C. Jégou, T. Delahaye *Inorg Chem* **2015**, *54*, 9749.
[11] C. Jégou, M. Gennisson, S. Peuget, L. Desgranges, G. Guimbretière, M. Magnin, Z. Talip, P. Simon *J. Nucl. Mater.* **2015**, *458*, 343.
[12] T.A. Olds, S.E. Karcher, K.W. Kriegsman, X. Guo, J.S. McCloy *J. Nucl. Mater.* **2020**, *530*, 151959.
[13] R. Mohun, L. Desgranges, C. Jégou, B. Boizot, O. Cavani, A. Canizarès, F. Duval, C. He, P. Desgardin, M.F. Barthe, P. Simon *Acta Mater.* **2019**, *164*, 512.
[14] G. Gutierrez, M. Bricout, F. Garrido, A. Debelle, L. Roux, C. Onofri *J. Eur. Ceram. Soc.* **2022**, *42*, 6633.
[15] A. Canizares, G. Guimbretière, Y.A. Tobon, N. Raimboux, R. Omnée, M. Perdicakis, B. Muzeau, E. Leoni, M.S. Alam, E. Mendes, D. Simon, G. Matzen, C. Corbel, M.F. Barthe, P. Simon *J. Raman Spectrosc.* **2012**, *43*, 1492.
[16] R. Mohun, L. Desgranges, J. Lechelle, P. Simon, G. Guimbretière, A. Canizarès, F. Duval, C. Jégou, M. Magnin, N. Clavier, N. Dacheux, C. Valot, R. Vauchy *Nucl. Instr. and Meth. in Phys. Res. B* **2016**, *374*, 67.
[17] L. Desgranges, A. Canizarès, P. Simon *J. Nucl. Mater.* **2022**, *559*.
[18] G. Gutierrez, C. Onofri, S. Miroa, M. Bricout, F. Leprêtre *Nucl. Instr. and Meth. in Phys. Res. B* **2018**, *434*, 45.
[19] L. Sarrasin, Y. Pipon, C. Gaillard, N. Moncoffre, N. Bérerd, P. Simon, D. Mangin, R. Ducher, M. Dubourg *Nucl. Instr. and Meth. in Phys. Res. B* **2018**, *435*, 111.
[20] D. Manara, B. Renker *J. Nucl. Mater.* **2003**, *321*, 233.
[21] H. He, D. Shoesmith *Phys. Chem. Chem. Phys.* **2010**, *12*, 8108.
[22] H. He, Z. Qin, D.W. Shoesmith *Electrochim. Acta* **2010**, *56*, 53.
[23] J.M. Elorrieta, L.J. Bonales, N. Rodriguez-Villagra, V.G. Baonza, J. Cobos *Phys. Chem. Chem. Phys.* **2016**, *18*, 28209.
[24] J.M. Elorrieta, L.J. Bonales, M. Naji, D. Manara, V.G. Baonza, J. Cobos *J. Raman Spectrosc.* **2018**, *49*, 878.
[25] H. He, Z. Ding, D.W. Shoesmith *Electrochim. Comm.* **2009**, *11*, 1724.
[26] J.M. Elorrieta, L.J. Bonales, S. Fernandez, N. Rodriguez-Villagra, L. Gutiérrez-Nebot, V.G. Baonza, J. Cobos *J. Nucl. Mater.* **2018**, *508*, 116.

[27] J.M. Elorrieta, A. Milena-Perez, J.-F. Vigier, L.J. Bonales, N. Rodriguez-Villagra *Phys. Chem. Chem. Phys.* **2022**, *24*, 28394.
[28] T. Livneh *J. Phys.: Condens. Matter* **2008**, *20*, 085202.
[29] B. Laskova, O. Frank, M. Zukalova, M. Bousa, M. Dracinsky, L. Kavan *Chem. Mater.* **2013**, *25*, 3710.
[30] C. Ciszak, M. Mermoux, G. Gutierrez, F. Leprêtre, C. Duriez, I. Popa, L. Fayette, S. Chevalier *J. Raman Spectrosc.* **2019**, *50*, 425.
[31] L. Sarrasin, S. Miro, C. Jégou, M. Tribet, V. Broudic, C. Marques, S. Peuget *J. Phys. Chem. C* **2021**, *125*, 19209.
[32] O. Kahraman, F. Lebreton, P. Martin, M. Mermoux *J. Appl. Phys.* **2022**, *132*, 115106.
[33] M.A. Mansouri, D.R. Olander *J. Nucl. Mater.* **1998**, *254*, 22.
[34] H. Matzke, A. Turos *J. Nucl. Mater.* **1983**, *113*, 249.
[35] T.B. Lindemer, T.M. Besmann *J. Nucl. Mater.* **1985**, *130*, 473.
[36] T.R. Griffiths, H.V. St.A. Hubbard *J. Nucl. Mater.* **1991**, *185*, 243.
[37] O.A. Maslova, G. Guimbretière, M.R. Ammar, L. Desgranges, C. Jégou, A. Canizarès, P. Simon *Material characterization* **2017**, *129*, 260.
[38] T. Livneh *Phys. Rev. B* **2022**, *105*, 045115.
[39] V.G. Keramidas, W.B. White *J. Chem. Phys.* **1973**, *59*, 1561.
[40] O.A. Maslova, X. Iltis, L. Desgranges, M.R. Ammar, C. Genevois, E.d. Bilbao, A. Canizarès, S.A. Barannikova, I.N. Leontyev, P. Simon *Material characterization* **2019**, *147*, 280.
[41] P.K. Morgan, T.A. Prusnick, M.A. Velez, K. Rickert, D.B. Turner, J.M. Mann *J. Raman Spectrosc.* **2021**, *52*, 1902.
[42] P.R. Graves *Appl. Spectrosc.* **1990**, *44*, 1665.
[43] J. Schoenes *J. Chem. Soc., Dalton Trans.* **1987**, *83*, 1205.
[44] T. Livneh, E. Sterer *Phys. Rev. B* **2006**, *73*, 085118.
[45] J.M. Elorrieta, L.J. Bonales, V.G. Baonza, J. Cobos *J. Nucl. Mater.* **2018**, *503*, 191.
[46] G. Guimbretière, L. Desgranges, A. Canizarès, G. Carlot, R. Caraballo, C. Jégou, P. Simon *Appl. Phys. Lett.* **2012**, *100*, 251914.
[47] P. Simon, A. Canizarès, N. Raimboux, L. Desgranges *MRS Bulletin* **2023**, *48*, 1.
[48] L. Desgranges, G. Baldinozzi, D. Simon, G. Guimbretière, A. Canizarès *J. Raman Spectrosc.* **2012**, *43*, 455.
[49] S. Bastians, G. Crump, W.P. Griffith, R. Withnall *J. Raman Spectrosc.* **2004**, *35*, 726.
[50] F. Colmenero, L.J. Bonales, J. Cobos, V. Timon *Spectroc. Acta A* **2017**, *174*, 245.
[51] L.J. Bonales, N. Rodriguez-Villagra, I. Sanchez-Garcia, O.R. Montoro *Prog. Nucl. Ener.* **2022**, *145*, 104122.
[52] G. Lu, A.J. Haes, T.Z. Forbes *Coord. Chem. Rev.* **2018**, *374*, 314.
[53] S.D. Senanayake, R. Rousseau, D. Colegrave, H. Idriss *J. Nucl. Mater.* **2005**, *342*, 179.
[54] J. Lv, G. Li, S. Guo, Y. Shi *J. Raman Spectrosc.* **2016**, *47*, 345.
[55] T. Shimanouchi, M. Tsuboi, T. Miyazawa *J. Chem. Phys.* **1961**, *35*, 1597.